Article

Gaussian-Based Machine Learning Algorithm for the Design and Characterization of a Porous Meta-Material for Acoustic Applications [†]

Alessandro Casaburo [1,*] , **Dario Magliacano** [1,2] , **Giuseppe Petrone** [1,2] , **Francesco Franco** [1,2]
and Sergio De Rosa [1,2]

1   WaveSet S.R.L., Via A. Gramsci 15, 80122 Naples, Italy; dario.magliacano@unina.it (D.M.);
    giuseppe.petrone@unina.it (G.P.); francof@unina.it (F.F.); sergio.derosa@unina.it (S.D.R.)
2   PASTA-Lab (Laboratory for Promoting Experiences in Aeronautical STructures and Acoustics), Department of
    Industrial Engineering-Aerospace Section, University of Naples "Federico II", Via Claudio 21,
    80125 Naples, Italy
*   Correspondence: alessandro.casaburo@unina.it
†   This paper is an extended version of our paper published in 50th International Congress and Exposition on
    Noise Control Engineering (Internoise 2021).

Abstract: The scope of this work is to consolidate research dealing with the vibroacoustics of periodic media. This investigation aims at developing and validating tools for the design and characterization of global vibroacoustic treatments based on foam cores with embedded periodic patterns, which allow passive control of acoustic paths in layered concepts. Firstly, a numerical test campaign is carried out by considering some perfectly rigid inclusions in a 3D-modeled porous structure; this causes the excitation of additional acoustic modes due to the periodic nature of the meta-core itself. Then, through the use of the Delany–Bazley–Miki equivalent fluid model, some design guidelines are provided in order to predict several possible sets of characteristic parameters (that is unit cell dimension and foam airflow resistivity) that, constrained by the imposition of the total thickness of the acoustic package, may satisfy the target functions (namely, the frequency at which the first Transmission Loss (TL) peak appears, together with its amplitude). Furthermore, when the Johnson–Champoux–Allard model is considered, a characterization task is performed, since the meta-material description is used in order to determine its response in terms of resonance frequency and the TL increase at such a frequency. Results are obtained through the implementation of machine learning algorithms, which may constitute a good basis in order to perform preliminary design considerations that could be interesting for further generalizations.

Keywords: Gaussian process; machine learning; artificial intelligence; porous foam; equivalent fluid; meta-material; inclusions; acoustics

1. Introduction

Present-day urbanization and traffic growth could seriously threaten human health, inducing annoyance, sleep disturbance, or even ischemic heart diseases [1], therefore the interest on environment noise reduction is quickly growing. In this context, porous media for acoustic purposes are materials made of channels, cracks, or cavities, in which sound waves pass through the foam and lose energy due to viscous and thermal effects [2,3]. However, porous media are not so efficient at low frequencies as they are at high ones [4]. Such limitation is generally bypassed through the use of multi-layer arrangements [5]; in any case, the effects of these solutions always rely on the allowable thickness or on the total mass of the soundproofing configuration [6,7].

In order to overcome such a constraint, low frequency performance of acoustic packages can be significantly enhanced by resorting to the use of porous media with embedded periodic inclusions acting as local resonators [8–10]. Such a configuration represents a

meta-material and provides proper dynamic filtering effects to the material, which could be beneficial for both the system dynamics and manufacturing. First proposed by Veselago [11] for electromagnetic waves, meta-materials have found, in recent years, a wide application in the acoustic field, since the insertion of artificial structural elements with periodic pattern allows one to control the propagation of wave phenomena [12]. Basically, the periodic geometry induces wave interference with constructive and destructive effects [13], which may lead to an enhancement of sound-absorbing properties with respect to traditional materials, such as porous ones [10].

Several types of meta-materials have been proposed in the relevant literature. For example, Yang et al. [14] introduce a decorated membrane, consisting of a pretensioned elastic membrane with rigid weights adhered on its surface; Mei et al. [15] obtain high sound absorption through a thin decorated membrane, while Yang et al. [16] investigate its upper bound. Moreover, Chen et al. [17,18] propose a complete analytical model for the absorption behavior of the membrane and confirm the energy absorption limit. Many works are inspired by Helmholtz resonators; for example, Fang et al. [19] combine several low-wavelength Helmholtz resonators in series in order to obtain an ultrasonic resonator; Wang et al. [20] propose an ultrathin open meta-material consisting in a large orifice in each unit cell; Kumar et al. [21] experimentally investigate a ventilated tunable acoustic meta-material to address the challenge of acoustical performance and ventilation efficiency in conventional noise barriers; and Wei et al. and Merkel et al. [22,23] demonstrate that Helmholtz resonators can exhibit monopolar resonances, in contrast to single decorated membranes, in which only dipole resonances occur. However, Yang et al. [24] show that a pair of coupled decorated membranes can provide monopolar resonances, too. The application of a shift cell technique, which is a reformulation of classical Floquet–Bloch conditions, is proposed by Magliacano et al. [25], which then consolidate the research concerning the acoustic performances of vibroacoustic treatments based on periodic patterns by embedding inclusions into a foam layer [26–28].

Nowadays, the use of meta-materials is suitable for different applications, such as energy, civil, and transportation (aerospace, automotive, and railway) engineering fields, where space, weight, and acoustic comfort still represent key aspects. For example, foam-based meta-materials find a wide range of applications in fuselage acoustic optimization, as reported by Magliacano et al. [29], which propose and investigate a meta-core solution made of a foam with cylindrical inclusions. However, in the same work it can be noted how the estimation of peculiar acoustic performance indicators of meta-materials, such as the percent increase of absorption coefficient or Transmission Loss (TL) peak when passing from a homogeneous medium to a material with embedded inclusions, lacks analytical formulation, therefore pushing towards the use of numerical simulations or experimental tests, with all that derives in terms of financial expenses, computational time, experimental setup, etc. For these reasons, it is reasonable to investigate alternative techniques, such as machine learning methods, which may be able to provide automated and quick estimations of the acoustic performances of meta-material packages, which may be useful in preliminary design phases or more advanced characterization tasks. Potentially, this may lead to noticeable money and time savings.

In particular, machine learning is a subset of Artificial Intelligence (AI) in which several disciplines, such as computational statistics, pattern recognition, image processing, data mining, adaptive algorithms, etc., converge. Machine learning methods allow a computational device to perform predictions in an automatic way by learning from a set of data and exploiting the information underneath, by improving the performances on a specific task from data without being explicitly programmed. A formal and more enlightening definition is given by Mitchell [30], which states that: "A computer program is said to learn from experience E with respect to some class of tasks T and performance measure P, if its performance at tasks in T, as measured by P, improves with experience E". The fact that there is not a task-specific algorithm, confers a high versatility to the approach, which allows its application in several research fields.

Thus, it is not surprising that recently, machine learning methods have received increasing attention dedicated to the analysis of the transmission and dispersion properties of periodic acoustic meta-materials, characterized by the presence of local resonators. Bianco et al. [31] and Michalopoulou et al. [32] provide interesting reviews on machine learning applied to acoustics. Novel functional applications in the optimal parametric design of smart tunable mechanical filters and directional waveguides involving the use of machine learning techniques are proposed by Bacigalupo et al. [33], as well as Gurbuz et al. [34], who use adversarial neural networks for the design of acoustic meta-materials, while the same topic is addressed, with cloaking as ultimate goal, by Shah et al. [35] through reinforcement learning. Both genetic algorithms and neural networks models are adopted in the literature [36], representing an effective approach in order to design acoustic meta-materials. In particular, as an efficient machine learning method, deep learning has been widely used for data classification and regression in recent years, showing good generalization performance [37]. Ciaburro and Iannace [38] train artificial neural networks with sound absorption coefficient measurements. Material properties are investigated by Stender et al. [39], which reverse-engineer sound absorbing materials in order to obtain features from the absorption coefficient.

In the present work, the effectiveness of machine learning methods as tools for performing the characterization is evaluated, in terms of TL peak frequency and percent increase (with respect to the homogeneous configuration) of meta-material acoustic packages in which the porous phase is described with two different models, namely, Delany–Bazley–Miki (DBM) and Johnson–Champoux–Allard (JCA) models. In particular, the proposed acoustic package is made of an arrangement of periodic porous unit cells with perfectly rigid inclusions.

When the DBM model is used, its simplicity allows to perform the analytical design of the meta-material assembly, which returns the unit cell dimension and the airflow resistivity on the basis of target thickness and resonance frequency; successively, the TL peak percent increase, with respect to the homogeneous configuration, is numerically estimated. Both the analytical and numerical procedures are used to generate the training set, after which the characterization of the meta-material is performed via a machine learning approach.

Successively, a similar characterization task is performed, in which the porous material is described with the JCA model, that is an acceptable trade-off between description accuracy of the material and model complexity. In more detail, in this task all the model's parameters (namely, unit cell dimension, porosity, airflow resistivity, tortuosity, viscous characteristic length, and thermal characteristic length) are provided as input features for machine learning methods, which predicts the resonance frequency of the TL peak, first, and the percent increase of the TL peak itself, then.

The use of two models describing a meta-material has a two-fold purpose: The investigation of machine learning prediction capabilities when a "simple" (DBM) and a "complex" (JCA) model is used, and the performance changes when the number of features and training samples vary according to the model. Indeed, the results prove that more complex material models allow a finer description in machine learning terms which leads to better results.

Gaussian processes are chosen as a machine learning method for this work, mainly due to their suitability to regression problems. In the second place, but not less importantly, Gaussian processes are mathematically equivalent to many well-known models (like Bayesian linear models) and are closely related to others, such as support vector machines. Moreover, the model provided is easier to handle and interpret than other counterparts and, at the same time, the method itself is easier to apply practically (it does not require plenty of decisions like architecture, activation functions, learning rate, etc.) [40,41].

Therefore, the aim of this work is to investigate the applicability of more manageable, practical, and interpretable machine learning methods, such as Gaussian processes, for the characterization of foam-based meta-materials, demonstrating, at the same time, the improvement of prediction performances, even though more complex phenomenological

material modeling is involved. Furthermore, the effectiveness in characterization tasks is also highlighted, which may boost up the preliminary phase of material design, characterization, and optimization, contextually reducing financial expenses and computational time related to experimental tests and numerical simulations.

This work is structured as follows. First of all, the theoretical frameworks related to the characterization of the meta-material, by means of DBM and JCA models (Sections 2.1.1 and 2.1.2, respectively), and to Gaussian processes (Section 2.2) are provided. Section 3 is dedicated to the analysis of results, in which data pre-processing and the application of the machine learning method are accomplished differently, according to the meta-material model. In particular, Section 3.1 illustrates the procedure that allows to analytically calculate the required values of foam airflow resistivity and unit cell dimension when the DBM model is considered. After this design part, in Section 3.2, the properties of the studied acoustic package are introduced, along with the 3-dimensional Finite Element (FE) geometries, and a parametric test campaign is performed for several setups, and test articles described with both the foam model. Successively, in Section 3.3, Gaussian processes are applied in order to predict the TL increases at the resonance frequencies when the meta-material is described by the DBM model; the resulting error is smaller than 5%. Then, the JCA equivalent fluid model is considered (Section 3.4), and Gaussian processes lead to even better results when using a smaller number of training examples, with respect to the DBM case. In Section 4, the results of this investigation are commented, and some possible future expansions of the present research are evaluated.

2. Theoretical Framework

This section provides the theoretical basis underlying the investigation executed in this work. Thus, it shortly introduces DBM and JCA models (Sections 2.1.1 and 2.1.2, respectively), used to describe the foam phase of the meta-material. The foam parameters vary in ranges of engineering interest (reported further in Table 1); thus, each set of parameters cannot be related to a specific material, but rather represents a material that can be realistically created and used in the engineering field. These parameters are used in Section 3 like features for the training of the machine learning method, namely Gaussian processes, which are presented in Section 2.2.

Table 1. Intervals of foam characteristics.

Foam Parameter	Interval	Model
Airflow resistivity, σ [kg/sm^3]	[1000, 87,000]	DBM, JCA
Unit cell dimension, d [m]	[0.01, 0.0950]	DBM, JCA
Transmission Loss (TL) peak frequency, f_{peak} [Hz]	[6276.346, 15,560]	DBM
Porosity, ϕ	[0.956, 0.99]	JCA
Tortuosity, α_∞	[1, 3]	JCA
Viscous characteristic length, λ_v [1/m]	[0.01, 0.294]	JCA
Thermal characteristic length, λ_{th} [1/m]	[0.1, 1]	JCA

2.1. Characterization of the Foam

The phase decoupling frequency is defined as the frequency for which the inertial effects of the solid phase are equal, in magnitude, to the viscous effects of the fluid part. If one considers a foam, excited by an acoustic load at a frequency much higher than the phase decoupling one, with a stiffness (or a weight) much greater than the one of the air, the material frame can be considered as rigid and motionless [42]. Therefore, the porous medium with motionless skeleton can be replaced by the homogeneous fluid layer without modifying the reflected field in the external medium [43]. Two classes of equivalent fluid models (that is expressions of complex density ρ and bulk modulus K as functions of the frequency and of the pore shape) can be listed [42]:

- Empirical models, which generally require the knowledge of a small number of parameters (or information); even if they are based on approximating assumptions, they are still very popular and very used;
- Semi-phenomenological models, which have been formulated for more complex pore morphologies; for this class of models, only the asymptotic behaviors are known, while a behavior between these asymptotes is assumed without being mathematically proven.

In this work, two models are considered: DBM, which is an empirical model, then JCA, which is a semi-phenomenological one.

2.1.1. Delany–Bazley–Miki (DBM) Model

Delany and Bazley [44] have proposed, on the basis of large measurements, empirical expressions for the values of the complex wave number k and characteristic impedance Z_c for forporous materials with porosities close to 1:

$$Z_c = \rho_0 c_0 \left[1 + 9.08 \left(10^3 \frac{f}{\sigma} \right)^{-0.75} - j11.9 \left(10^3 \frac{f}{\sigma} \right)^{-0.73} \right], \tag{1}$$

$$k = \frac{\omega}{c_0} \left[1 + 10.8 \left(10^3 \frac{f}{\sigma} \right)^{-0.7} - j10.3 \left(10^3 \frac{f}{\sigma} \right)^{-0.59} \right], \tag{2}$$

where ρ_0 is the density of air, c_0 is the speed of sound in air, f is the frequency, and ω is the angular frequency. Boundaries, proposed by the authors, for the validity of these power law expressions are $0.01 < \frac{f}{\sigma} < 1.00$. This empirical model, which can provide reasonable estimations of k and Z_c in the approximate frequency range defined above, is still widely used for its simplicity: Only one parameter, the airflow resistivity σ, is needed to describe the acoustic behavior of a material.

The model by Delany–Bazley–Miki (DBM) [45] presents revised expressions for the complex wave number k and characteristic impedance Z_c of the Delany–Bazley model [44]. In the case of multi-layers, Miki noticed that the real part of the surface impedance, when estimated with the classical Delany–Bazley model, may turn negative at low frequencies, thus leading to a non-physical result. In this context, Miki suggests the usage of the following expressions:

$$Z_c = \rho_0 c_0 \left[1 + 5.5 \left(10^3 \frac{f}{\sigma} \right)^{-0.632} - j8.43 \left(10^3 \frac{f}{\sigma} \right)^{-0.632} \right], \tag{3}$$

$$k = \frac{\omega}{c_0} \left[1 + 7.81 \left(10^3 \frac{f}{\sigma} \right)^{-0.618} - j11.41 \left(10^3 \frac{f}{\sigma} \right)^{-0.618} \right]. \tag{4}$$

The validity of Miki model is the same of that related to the original formulation, even if his revised expressions behaves well in a larger frequency range, in particular for $\frac{f}{\sigma} < 0.01$.

2.1.2. Johnson–Champoux–Allard (JCA) Model

The JCA model is based on the work by Johnson, Koplik, and Dashen [46], describing the visco-inertial dissipative effects inside porous media through a semi-phenomenological model characterized by the complex density of an acoustical porous material with a motionless skeleton having arbitrary pore shapes:

$$\rho(\omega) = \frac{\alpha_\infty \rho_0}{\phi} \left(1 + \frac{\sigma \phi}{j\omega \rho_0 \alpha_\infty} \sqrt{1 + \frac{4\alpha_\infty^2 \eta \rho_0 \omega}{\sigma^2 \Lambda^2 \phi^2}} \right). \tag{5}$$

Successively, on the basis of this research, Champoux and Allard [47] formulated an expression for the equivalent bulk modulus for the same type of foams:

$$K(\omega) = \dfrac{\dfrac{\gamma P_0}{\phi}}{\gamma - (\gamma - 1)\left[1 - j\dfrac{8\kappa}{\Lambda'^2 c_p \rho_0 \omega}\sqrt{1 + j\dfrac{\Lambda'^2 c_p \rho_0 \omega}{16\kappa}}\right]^{-1}},\qquad(6)$$

where γ is the fluid specific heat ratio, P_0 is the fluid equilibrium pressure, ϕ is the porosity, κ is the thermal conductivity of the air, Λ' is the characteristic dimension, and c_p is the fluid specific heat at a constant pressure.

Equation (6) does not represent the exact behavior of the equivalent bulk modulus when the angular frequency ω approaches low values. At low frequencies, the real part approaches asimptotically to the unit value, representative of an isothermal process; at high frequencies, it approaches the value 1.4, indicating an adiabatic process. In both cases, the imaginary part approaches zero.

2.2. Gaussian Processes

Stochastic processes can be briefly defined as the generalization of random variables to functions. More precisely, they are collections of random variables indexed by the input vector $\mathbf{x}$ [41]. Thus, if $\mathbf{x}_1, \mathbf{x}_2, \ldots, \mathbf{x}_N$ are the d-dimensional training data points, a process is defined by the joint probability density of any finite subset $(Y(\mathbf{x}_1), \ldots, Y(\mathbf{x}_k))$ (with $k < N$). A Gaussian process is a stochastic process whose joint density function is Gaussian and, therefore, completely defined by its mean and co-variance [48–51].

If the training data set is made of n ordered pairs $(\mathbf{x}_1, t_1), \ldots, (\mathbf{x}_n, t_n)$, where t_i is a sample from a random variable $T(\mathbf{x}_i)$, then a prediction T^* at a new input $\mathbf{x}^*$ is given by the conditional distribution $p(T^*|T_1, \ldots, T_N)$. It can be demonstrated that the predicted mean and co-variance at $\mathbf{x}^*$ are given by [41]:

$$E[T^*] = \mathbf{k}^* \mathbf{K}^{-1}\mathbf{t},\qquad(7)$$

$$var[T^*] = \mathbf{k}^* - \mathbf{k}^T \mathbf{K}^{-1}\mathbf{k},\qquad(8)$$

where $\mathbf{k}$ denotes the co-variance vector of the training set (TS), k^* denotes the co-variance of the new input $\mathbf{x}^*$, $\mathbf{K}$ denotes the co-variance matrix, and $\mathbf{t}$ denotes the vector of the samples from the random variable $\mathbf{x}_i$).

For simplicity, it is assumed that the Gaussian process has zero mean, therefore it is necessary to define just the co-variance between two points $\mathbf{x}$ and $\mathbf{x}'$; this is done with the co-variance function $C(\mathbf{x}, \mathbf{x}')$. Such a function is a crucial element in a Gaussian process predictor, as it encodes the assumptions about the function to learn in terms of similarity between data points (close points are more likely to have similar target values, hence training points close to a test points should be informative about the prediction at that point).

The co-variance function chosen in this work is the squared exponential. This function is infinitely differentiable, thus very smooth [40]. Even though some authors, such as Stein [52], argue that such a smoothness is unrealistic, therefore recommending the Matérn class of covariance functions, the squared exponential function is an excellent trade-off among code implementation, hyperparameters evaluation, and interpretation, which explains why it is probably the most used [40]. In fact, this type of covariance function basically represents the exponential of a weighted squared distance between points in $\mathbb{R}^d$, so that vectors close in the input space give rise to highly correlated outputs:

$$C(\mathbf{x}^{(i)}, \mathbf{x}^{(j)}) = v_0 e^{\left[-\frac{1}{2}\sum_{l=1}^{d} a_l (x_l^{(i)} - x_l^{(j)})^2\right]} + b.\qquad(9)$$

The term v_0 controls the amplitude of the process, and b is a bias term related to the vertical offset. The term a_l weighs the importance of the dimension under consideration (for example, if it is small, then the l-th input is down-weighted).

Obviously, it is unrealistic to assume the knowledge of all the co-variance parameters *a priori*. It is, therefore, useful to start with a guess and adapt the values of these parameters to the training data set. This operation is carried out by means of scaled conjugate gradient optimization [41], which suitably modulates the co-variance parameters once a random, initial guess is provided.

3. Analyses and Results

This section describes the analyses performed and the results obtained; Figure 1 is a useful reference for better understanding the steps of the characterization procedure involving DBM model, explained in the following sub-sections. The other characterization task models the porous phase with the JCA model.
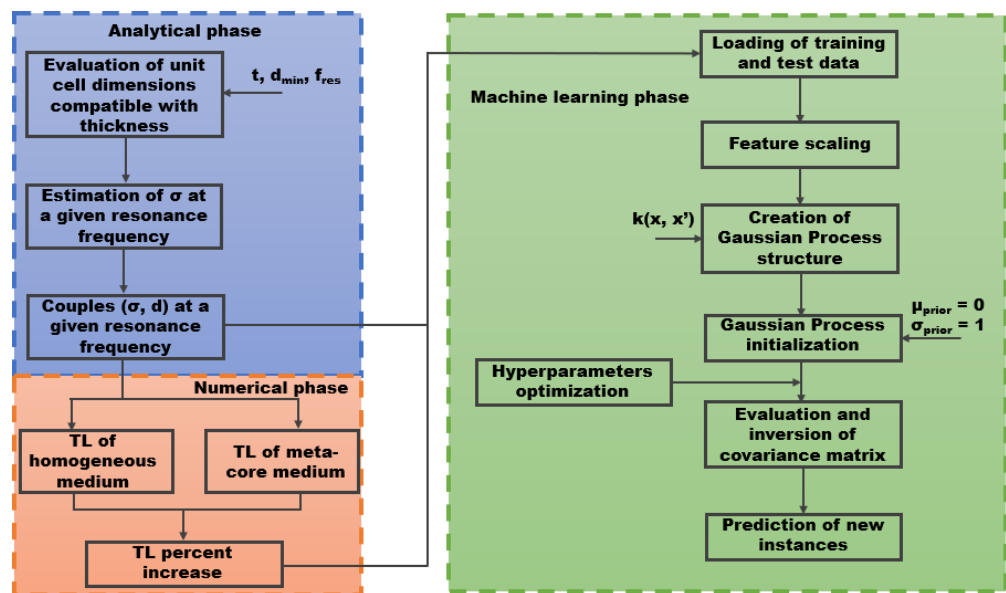
Figure 1. Flowchart of the design task concerning meta-materials described with the DBM model. As illustrated, the blue, red, and green sections are related to the activities executed in the analytical, numerical, and machine learning phases.

3.1. Analytic Part: Calculation of the Periodic Resonance Frequency

Firstly, the DBM model is used to describe the porous medium. This Section reports the analytical design procedure which, for fixed thickness and resonance frequency, returns the unit cell dimension and airflow resistivity of the model. In particular, it is illustrated how Equation (4) is inverted in order to estimate the required foam airflow resistivity σ for a desired resonance frequency. First of all, it should be pointed out that the resonance physics that is exploited herein, is linked to the well-known phenomenon that occurs when half the wavelength is equal to the periodicity dimension (namely, the unit cell dimension). So told, Equation (4) essentially involves four quantities: The wavenumber k, the frequency f (and thus the angular frequency $\omega = 2\pi f$), the speed of sound in air c_0 (that, in this context, can be considered as a constant value), and the foam airflow resistivity σ. Normally, such quantities are linked to each other such that the first one is the output, while the others are treated as inputs. In order to explicit the wavelength λ, which is required for the aforementioned reason, the wavenumber k is expressed as $k = \frac{2\pi}{\lambda}$; then, since in correspondence of a periodic resonance, it is verified that the dimension of periodicity, d, is given by [25,26]:

$$d = \frac{\lambda}{2},\tag{10}$$

in that case one may write that $k = \frac{\pi}{d}$. At this point, considering that the real part of a complex wavenumber is generally linked to the propagation of the wave, while the imaginary one is related to its dissipation, for the purpose of the present analysis only

the real part may be taken into account. Therefore, by neglecting the imaginary part of Equation (4) and applying the aforementioned substitutions, in correspondence of a periodic resonance one obtains:

$$\sigma = 36.1 f \left(\frac{c_0}{2df} - 1 \right)^{1.618}. \tag{11}$$

The code used for this design phase, written in MATLAB, is based on Equation (11) and initially asks for two geometrical constraints: The total available thickness, and the minimum unit cell dimension, which could be restrained by manufacturing aspects, and thus is limited by both lower and upper boundaries; furthermore, the prompt also requires the input of a target resonance frequency, which could fall in the whole audible range. Then, starting from the combination of the two geometrical constraints, the scripts calculates the possible numbers (and thus dimensions) of unit cells along the thickness; for each of them, the required σ at the assigned resonance frequency is computed through Equation (11). In this configuration, the script may display one or more (or even none) possible combinations of unit cell dimensions and airflow resistivity that, from a practical point of view, may lead to the choice respectively of a specific periodic pattern and foam material, with the aim of obtaining an acoustic resonance at the desired frequency.

3.2. Finite Element Part: Parametric Analysis about Airflow Resistivity and Periodicity Dimension

This Section provides the details of the FE model used to simulate the meta-material, creating both the training and test sets: The outcomes of the analytical design phase, for the DBM model, or the material parameters, for the JCA model, are provided to the FE software, which returns TLs of a homogeneous and a meta-core medium, allowing to evaluate the TL peak percent increase. These results, along with the airflow resistivity and unit cell dimension are then passed to the machine learning algorithm.

The details of the FE simulations (geometry, mesh size, number of elements, and number of nodes) used for modeling do not change whether the DBA or JCA model is used; the only difference is in the type and number of input parameters. Moreover, the foam characteristics (airflow resistivity, porosity, unit cell dimension, tortuosity, viscous, and thermal characteristic lengths), which are variable in order to generate the training and test sets, are restrained into intervals of engineering reasonability of common industrial foams. These intervals are summarized in Table 1. The first columns reports the foam parameter, the second column lists the value intervals, and the third columns indicates the model for which they are used as input features in the machine learning phase.

The FE model is constituted by a layer of foam, with embedded periodic inclusions with the shape of cylindrical holes with perfectly rigid walls (Figure 2); the choice of the inclusion geometry represent an example, and may eventually impact the amplitude and/or the shape of the TL resonance peak, but not its frequency (since this only depends on the foam properties and on the dimension of the periodicity). For what concerns the FE implementation, the module "Pressure Acoustics and Frequency Domain" of COMSOL MultiPhysics is used both as a modeling environment and numerical solver. For all structures presented in this work, the mesh consists of tetrahedral elements, generated through physics-controlled algorithms that are pre-implemented in the software. Nevertheless, the authors verified that the maximum element size of each HR meshed is always lower than $1/4$ of the minimum wavelength λ, which leads to an average number of elements through models with different sizes approximately equal to 14,250. Since the analyses are carried out considering an excitation consisting of a normal incidence plane wave acting on a layer of air (whose properties are reported in Table 2) along the *z*-axis, the only fundamental boundary condition to apply is the so-called Perfectly Matched Layer (PML) on the very bottom face of the models. Indeed, this represents an artificial absorbing layer for wave equations, commonly used to truncate computational regions in numerical methods in order to simulate problems with open boundaries; this allows the PML to strongly absorb outgoing waves from the interior of a computational region, without reflecting them back

into the interior. On the contrary, boundary conditions applied on faces normal to the *x*- and *y*- axes are not relevant for analyses with the above-mentioned kind of excitation, since under this condition the waves do not have propagating components along those directions; thus, for the sake of computational simplicity, a Sound Hard Boundary Wall (SHBW) boundary condition is applied herein. Eventually, for different angles of excitation, proper periodic conditions should be used instead.
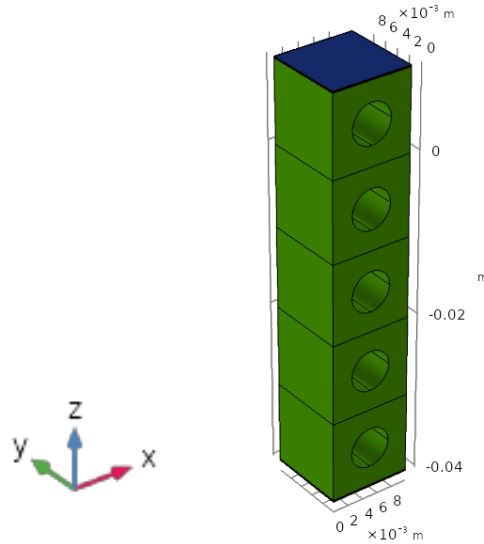
Figure 2. Example of FE geometry with five unit cells along the foam core thickness; the foam is green–colored, while the layers of air are blue–colored.

Table 2. Properties of air.

Density, ρ_0 [kg/m³]	1.213
Speed of sound, c_0 [m/s]	3.42×10^2

For a plane wave configuration at normal incidence $\theta = \phi = 0$, and thus oriented towards the negative direction of *z*-axis, the TL is computed as reported in Equation (12):

$$\text{TL} = 10\log_{10}\frac{\Pi_{incident}}{\Pi_{transmitted}}. \tag{12}$$

In the context of this work, the TLs related to the homogeneous (which, obviously, has no inclusions) and the meta-core models are respectively estimated through a TMM implementation [43] of Equations (13) and (14), and an FE solution of Equation (12).

$$\text{TL} = 10\log_{10}(\frac{1}{4}|T_{11} + \frac{T_{12}}{\rho_0 c_0} + \rho_0 c_0 T_{21} + T_{22}|^2), \tag{13}$$

$$\text{with } \begin{bmatrix} T_{11} & T_{12} \\ T_{21} & T_{22} \end{bmatrix} = \begin{bmatrix} \cos(kd) & \text{j}\sin(kd)Z_c \\ \frac{\text{j}\sin(kd)}{Z_c} & \cos(kd) \end{bmatrix}. \tag{14}$$

A parametric analysis is performed for all possible combinations of two chosen sets of foam airflow resistivity and unit cell dimension values. In particular, 12 airflow resistivities and 10 unit cell dimensions are selected (refer to Table 1 for the ranges), both on a logarithmic scale, for a total of 120 different test cases; for each of them, the periodic resonance frequency (Figure 3) is analytically calculated through the approach illustrated in Section 3, while the TL percentage increase (Figure 4) related the meta-core solution,

compared to its homogeneous counterpart at fixed total thickness, is numerically estimated in the COMSOL environment using Equations (12) and (13).
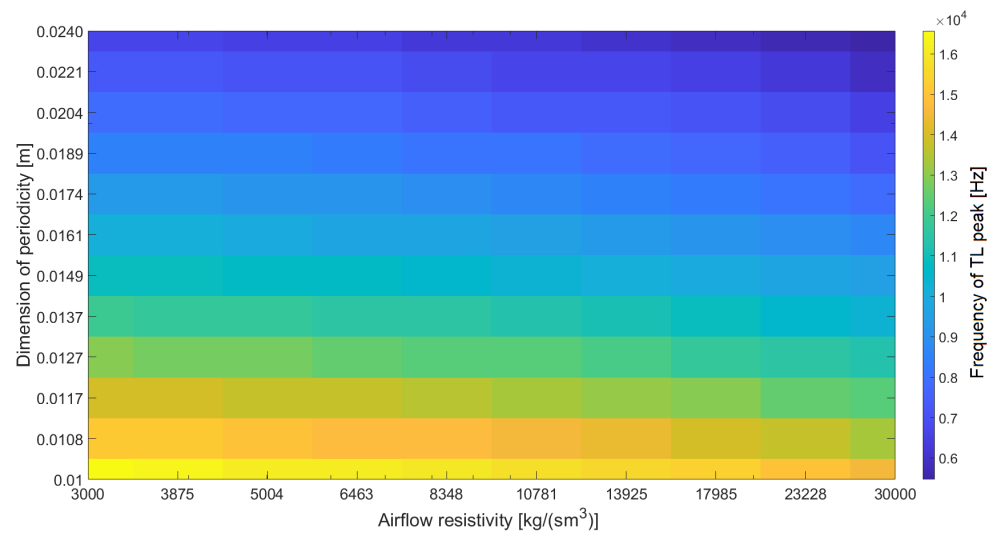
Figure 3. Transmission Loss peak frequency behavior as a function of unit cell dimension and foam airflow resistivity.
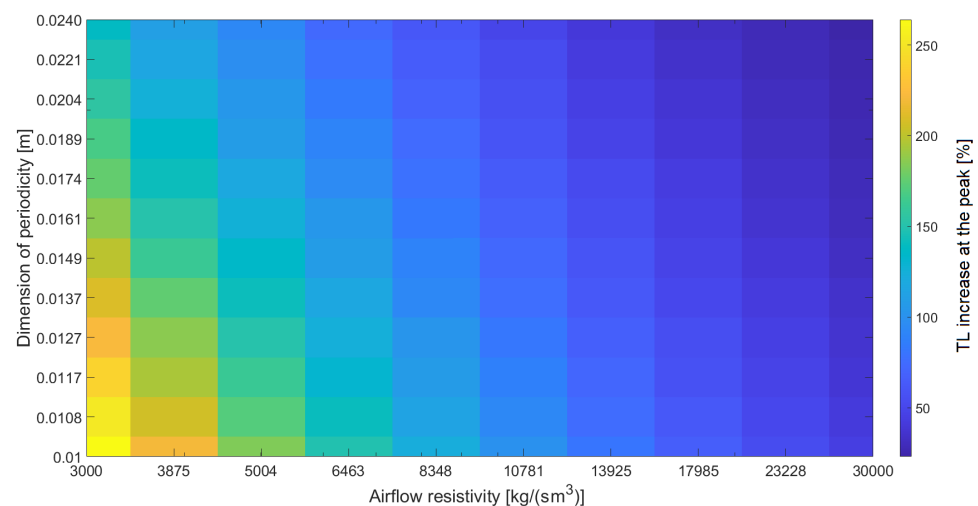
Figure 4. Transmission Loss peak amplitude behavior as a function of unit cell dimension and foam airflow resistivity.

For example, considering a couple of σ and d values respectively equal to 5004 kg/(sm^3) and 0.0127 m, from Figure 3 a resonance frequency of around 13,000 Hz (the analytical value is 12,735 Hz) may be found, while from Figure 4 an increase in the TL amplitude peak of around 150% (the FE value is 151%) may be estimated; instead, considering a couple of σ and d values respectively equal to 17,985 kg/(sm^3)] and 0.0189 m, from Figure 3, a resonance frequency of around 8000 Hz (the analytical value is 7689 Hz) may be found, while from Figure 4, an increase in the TL amplitude peak of around 50% (the FE value is 40%) may be estimated.

3.3. Machine Learning Part: Prediction of the Transmission Loss Increase at the Resonance Frequency (DBM Model)

The objective of this Section is to analyze the performance capabilities of Gaussian processes when predicting the TL percent increase of meta-materials (with respect to the equivalent homogeneous configuration). As already stated in Section 2.2, the predictions

on new instances are given by Equation (7), and the estimation of the hyper-parameters is carried out with an optimization algorithm. Therefore, once the co-variance function is decided, Gaussian processes do not need any user-defined choice other than the number of training examples. Figure 1 summarizes the several steps occurring in this phase.

Since the generation of both a numerical and/or experimental training set would be time consuming and financially expensive, there is an attempt to carry out the prediction of new instances by using the lowest number of training examples as possible; such a prediction would be considered satisfying if the percent error between the numerical and predicted peak reduction is below 5%. Moreover, in order to demonstrate the robustness of the method with the chosen number of examples, in the problem at hand, the predictions are made with three different training sets, called TS1, TS2, and TS3. To this aim, the 120 test cases numerically obtained are used as pool from which to extract training and test examples. In particular, the complete observation of each sample is made of four features: Airflow resistivity, unit cell dimension, and resonance frequency as input, while the TL peak decrease is, obviously, the output. The three sets share 20 samples, which describe the boundaries of the input space (to avoid extrapolation), to which other examples are randomly added from the aforementioned pool. The remaining elements are used for testing the generalization capabilities of the method.

Before proceeding with the learning, feature scaling is executed on all the training samples as:

$$x'_i = \frac{x_i - \mu}{\sigma_{std}}, \tag{15}$$

where x_i and x'_i are the original i-th feature and the scaled one, respectively, μ is the mean value of the feature, and σ_{std} is the standard deviation of the feature, both evaluated on the whole training set. This operation is almost mandatory, since the different orders of magnitude of the parameters involved may generate numerical problems during learning. Feature scaling, instead, reduces all the features to the same order of magnitude. After learning, the features are then descaled, so that the results of the predictions are made understandable to the user.

The results provided by Gaussian processes are summarized in Figure 5. Each row displays, on the left, a 3D plot relating the three inputs (airflow resistivity, unit cell dimensions, and resonance frequency), on the cartesian axis, and the predicted peak decrease (color-coded) corresponding to each coordinate. On the right, 2D plots link the independent variables (σ, d) (which provide frequency according to Equation (4)) to the corresponding prediction error. In these figures, the black dots indicate the training examples, that must not be considered for the performance evaluation of the machine learning method.

Concerning these performances, the 2D plots show that, with a training set made of 45 samples, the prediction error remains inside the 5% boundary. The distribution of the higher errors does not follow a predictable pattern, since they not only appear in the central region of the map, but are also close to the boundaries and, sometimes, training examples. However, the same considerations hold for the lower errors.
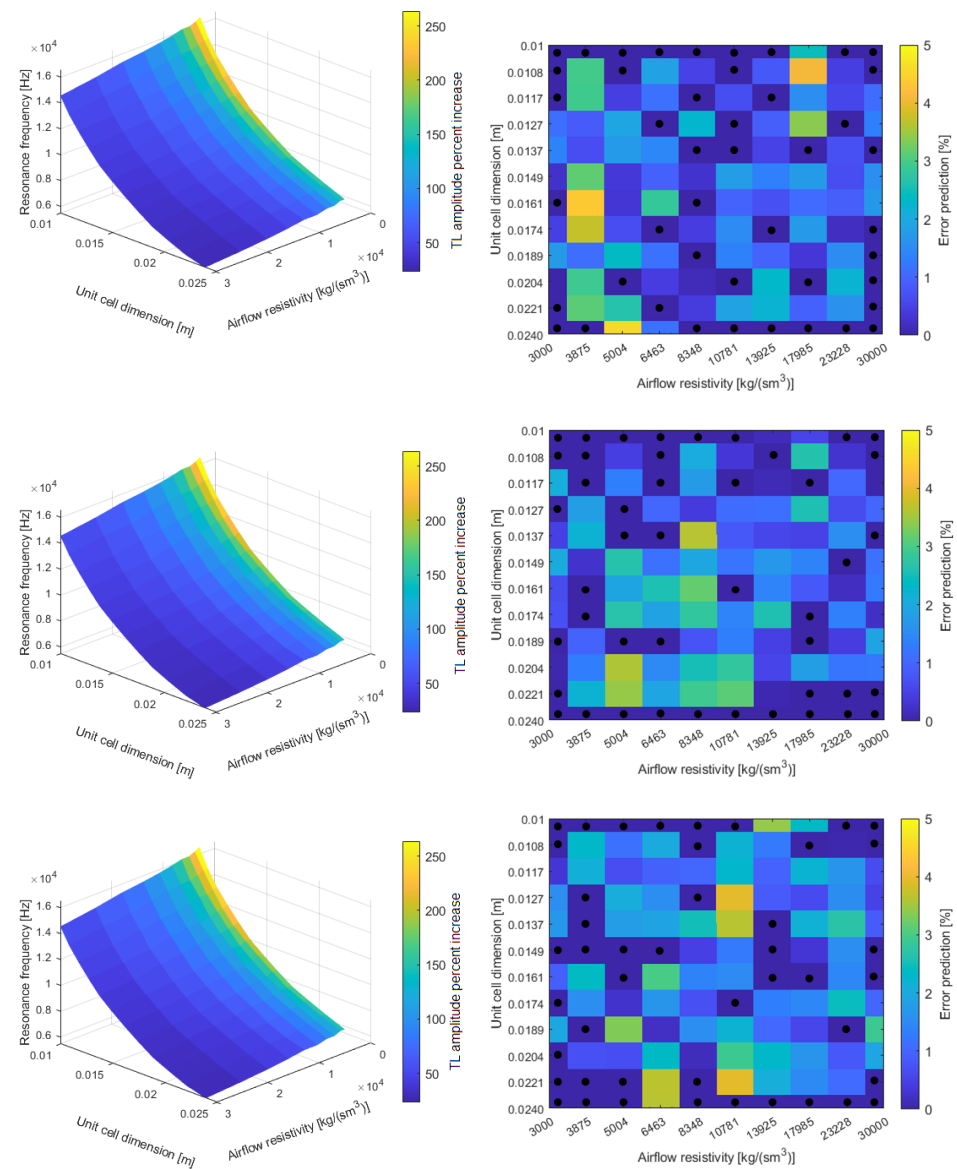
Figure 5. On the left, from top to bottom, 3D plots that relate the three inputs of the machine learning algorithm to the predicted TL amplitude percentage increase at the resonance peaks (coded in the colorbar), for each of the three tested TSs. On the right, from top to bottom, 2D plots that relate the two mutually independent inputs of the machine learning algorithm to the percentage error about the prediction of TL amplitude percentage increase at the resonance peaks (coded in the colorbar), for each of the three tested TSs; values marked with black points are those used as training set, while all the remaining ones constitute the actual test set.

In order to have greater insight on the performances of Gaussian processes, three test cases are considered: The analytical and numerical TL curves are provided in Figure 6 (where the resonance frequency axis is cut at 14,000 Hz, in order to better visualize the curves and the related peaks), while Table 3 summarizes the results in terms of reference amplitude, predicted amplitude, and prediction error for all the three training sets. Table 3 highlights the excellent performances of Gaussian processes. More generally, TS1, TS2, and TS3 exhibit a mean percent error equal to 1.49, 1.42, and 1.66, respectively, which is much lower than the 5% boundary fixed.
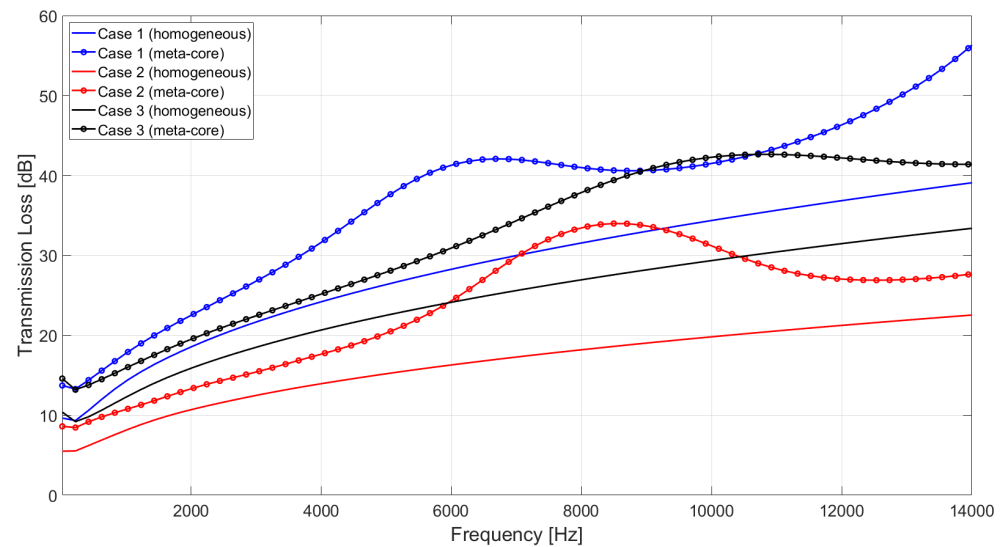
Figure 6. Transmission Loss analytically (homogeneous) and numerically (meta-core) computed, respectively through TMM and FE approaches, for three test cases with different combinations of airflow resistivity and unit cell dimension; further details about Case 1, Case 2, and Case 3 are reported in Table 3. The TL percent increase is estimated on meta-core curves, using the homogeneous curves as reference.

Table 3. Amplitude increments at the resonance peaks and related errors for three tested (σ, d) couples, predicted with machine learning through three different training sets (ML-TS).

	Case 1	Case 2	Case 3
(σ, d)	(13,925, 0.022)	(8348, 0.0174)	(23,228, 0.0137)
Resonance frequency [Hz]	6680	8900	10,515
Amplitude increment (FEM) [%]	42.38	78.09	42.17
Amplitude increment (ML-TS1) [%]	42.32	79.22	41.61
Error on amplitude increment (ML-TS1) [%]	0.13	1.44	1.33
Amplitude increment (ML-TS2) [%]	42.66	79.42	41.72
Error on amplitude increment (ML-TS2) [%]	0.66	1.70	1.06
Amplitude increment (ML-TS3) [%]	42.69	79.40	41.31
Error on amplitude increment (ML-TS3) [%]	0.72	1.67	2.04

3.4. Machine Learning Part: Prediction of the Resonance Frequency and Transmission Loss Increase at the Resonance Frequency (JCA Model)

The second characterization task is performed with a meta-material whose foam phase is described by the JCA model. This time, there is no analytical phase, only numerical simulations are executed in order to generate training and test sets. The input features are unit cell dimension, porosity, airflow resistivity, tortuosity, viscous characteristic length, and thermal characteristic length; the output features are TL peak frequency and percent increase. Section 3.4 reports the results of Gaussian processes applied to meta-materials

described with JCA models. In this Section, Gaussian processes are used to predict the resonance frequency and TL percent increase (at the predicted resonance frequency) of meta-materials described with the JCA model.

The JCA model allows to describe a meta-material in terms of six variables, namely: Unit cell dimension d, porosity ϕ, airflow resistivity σ, tortuosity α_∞, viscous characteristic length λ_v, and thermal characteristic length λ_{th}. From a machine learning point of view, such a plethora of parameters is useful fo reducing the number of training samples, thus it is expected that good predictions can be obtained with a limited number of examples for the training phase. The number of training examples is 38. Due to the high dimensionality of feature space, the description of its boundaries with samples, as performed in Section 3.3, in order to avoid extrapolation, cannot be done since it would require the description of a six-dimensional hypervolume (and would require much more examples than those available).

The first application implies the use of a number of training examples as much as possible close to that used with the DBM model, which is 45, in order to compare the performance of the same machine learning algorithm when all other variables are retained. Thus, all the training samples are used (that is, 35), except three, used for the test phase. The input values of the test samples are reported in Table 4, while the predictions provided by Gaussian processes, for three different training, are summarized in Tables 5 and 6 for the resonance frequency and the TL peak percent increase, respectively.

Table 4. Input values of test samples.

d [m]	ρ	σ [kg/sm^3]	α_∞	λ_v [1/m]	λ_{th} [1/m]
0.0425	0.971	19,360	2.16	0.024	0.458
0.0650	0.956	3490	1.06	0.187	0.25
0.0950	0.98	9500	1.01	0.166	0.249

Table 5. Predictions of resonance frequency (in Hz) with 35 training examples.

	Test Sample 1	Test Sample 2	Test Sample 3
Reference	2724	2523	1719
Prediction 1	2724	2523	1718.9
Percent error 1	0.0016%	5.6×10^{-4}%	0.0039%
Prediction 2	2723.9	2522.7	1719.3
Percent error 2	0.0035%	0.0102%	0.0186%
Prediction 3	2723.6	2522.7	1718.5
Percent error 3	0.0142%	0.0131%	0.0318%

Table 6. Predictions of TL peak percent increase with 35 training examples.

	Test Sample 1	Test Sample 2	Test Sample 3
Reference	45%	157%	25%
Prediction 1	45%	157%	25%
Percent error 1	0.0025%	0.0074%	0.0028%
Prediction 2	45%	157.02%	26%
Percent error 2	0.0065%	0.0152%	0.0095%
Prediction 3	44.85%	156.77%	25.95%
Percent error 3	0.329%	0.144%	0.193%

The results highlight the high accuracy of the predictions the Gaussian processes are capable of providing. Comparing these outcomes with those obtained with the DBM model, since both the characterization of the Gaussian process and the number of training samples are the same (or, more precisely, the number of training samples is almost the same, being even smaller for the JCA case), it is clear that the main cause behind this improvement of performances is due to the finer characterization allowed by the JCA model, providing six input features against three in the case of the DBM model.

Hence, it is reasonable to continue the investigation in order to understand the change of the performances of the machine learning algorithm when reducing the number of training examples. Quite surprisingly, it is possible to reduce the training set to 5 samples (less samples would bring to numerical errors in the procedure) and still obtain the same quality of results, as highlighted in Tables 7 and 8, reporting the predictions and errors of the same test samples.

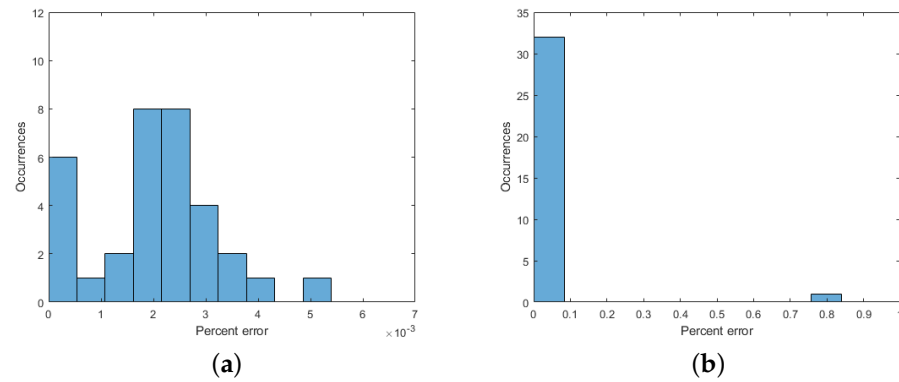**Table 7.** Predictions of resonance frequency (in Hz) with five training examples.

	Test Sample 1	Test Sample 2	Test Sample 3
Reference	2724	2523	1719
Prediction 1	2724	2523	1719
Percent error 1	1.71×10^{-4}%	7.04×10^{-4}%	0.0017%
Prediction 2	2724	2523	1718.9
Percent error 2	2.93×10^{-4}%	7.17×10^{-4}%	0.0048%
Prediction 3	2723.9	2522.9	1718.9
Percent error 3	0.0043%	0.0051%	0.0054%

Table 8. Predictions of TL peak percent increase with five training examples.

	Test Sample 1	Test Sample 2	Test Sample 3
Reference	45%	157%	26%
Prediction 1	45%	156.98%	26%
Percent error 1	0.0032%	0.0118%	0.0030%
Prediction 2	45.12%	157.03%	26.08%
Percent error 2	0.2749%	0.0177%	0.3226%
Prediction 3	44.96%	156.91%	26.01%
Percent error 3	0.0870%	0.0605%	0.0421%

Also in this case, the predictions accuracy is very high, exhibiting a very small percent error. Moreover, a larger picture concerning the distribution of errors (in the case of the third training) in the remaining 30 test samples is provided by the histograms in Figure 7.

The histograms show that, in general, the errors are very low for all the other test samples. Particularly, the errors in predicting the resonance frequency are mainly concentrated in the interval 0–4×10^{-3}%, while those obtained when predicting the TL peak increase are almost totally in the interval 0–0.08%.

(a)

(b)

Figure 7. Histograms of the percent prediction errors occurrences when predicting the resonance frequency (**a**) and the TL percent peak increase (**b**) with five training examples; these distributions are evaluated on the third training. Each bin contains three occurrences.

The last test on the performances of Gaussian processes is performed by using five training examples and removing the porosity as feature from the training set, since its values do not change significantly and, more generally, it is proven that it does not affect very much the acoustic behavior of meta-materials described with the JCA model. The predictions of the usual three test samples are listed in Tables 9 and 10, and the error histograms are displayed in Figure 8.

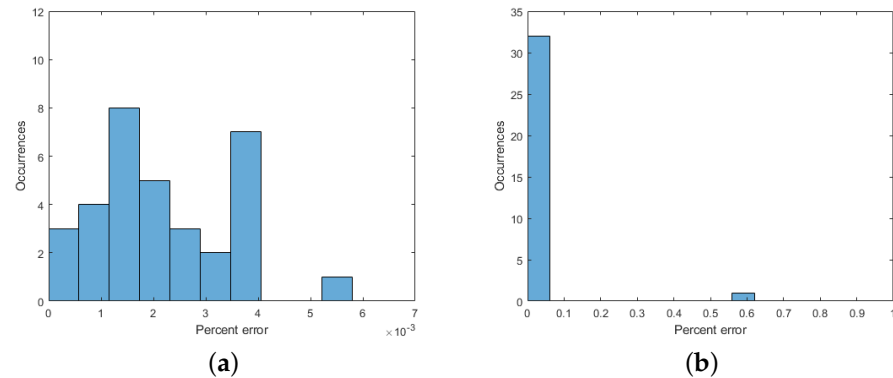**Table 9.** Predictions of resonance frequency (in Hz) with five training examples and without porosity.

	Test Sample 1	Test Sample 2	Test Sample 3
Reference	2724	2523	1719
Prediction 1	2724	2523	1719
Percent error 1	0.0012%	0.0016%	0.0016%
Prediction 2	2724	2523	1718.9
Percent error 2	0.0013%	6.26×10^{-4}%	0.0081%
Prediction 3	2723.9	2522.9	1718.8
Percent error 3	0.0039%	0.0031%	0.0119%

Table 10. Predictions of TL peak percent increase with five training examples and without porosity.

	Test Sample 1	Test Sample 2	Test Sample 3
Reference	45%	157%	26%
Prediction 1	45.01%	157.01%	26.01%
Percent error 1	0.0187%	0.0091%	0.0209%
Prediction 2	45%	156.98%	26%
Percent error 2	0.0016%	0.0143%	0.0019%
Prediction 3	45%	156.98%	26%
Percent error 3	0.0017%	0.0116%	0.0051%

The results, still excellent, highlight that removing porosity does not affect significantly the performances of Gaussian processes. In particular, focusing on the histograms, the distribution of errors is mainly concentrated in the interval 0–4×10^{-3}% for resonance frequency, and still in the interval 0–0.08% for TL percent peak increase. These outcomes demonstrate that removing a feature, which has negligible effects in the analytical model,

has, actually, a corresponding outcome in the performances of machine learning algorithms. This may be used as a guideline in the choice of features for describing observations in future applications of machine learning methods.

Figure 8. Histograms of the percent prediction errors occurrences when predicting the resonance frequency (**a**) and the TL percent peak increase (**b**) with five training examples and without porosity; these distributions are evaluated on the third training. Each bin contains three occurrences.

4. Conclusions

The scope of this work is to develop and validate tools for boosting up the characterization of vibroacoustic packages based on foam cores with embedded periodic patterns through the implementation of machine learning algorithms.

First of all, the theoretical frameworks related to the characterization of the meta-material and to the chosen machine learning method are provided. Then, a procedure that allows to analytically calculate the required values of foam airflow resistivity and unit cell dimension in order to reach a desired target in terms of periodic resonance frequency is illustrated under specified constraints. Successively, the properties of the studied acoustic package are introduced, together with the 3-dimensional finite element geometries, and a parametric test campaign is performed for several setups, each with different values of foam airflow resistivity and unit cell dimension. In conclusion, a Gaussian-based machine learning algorithm is developed and applied in order to predict, with an error smaller than 5%, the Transmission Loss increases at the resonance frequencies when the DBM model is used to describe the meta-material. When the JCA model is considered, the Gaussian process can provide even better results, in predicting resonance frequencies and TL peak percent increases, with much less training examples, by increasing the number of features characterizing the observations.

Therefore, machine learning methods that are easy to handle and interpret, such as Gaussian processes, provide several advantages when meta-materials packages need characterization. In fact, the switch from DBM to JCA models demonstrates that the increase of input features leads to a noticeable reduction of the number of training examples. Hence, if one wants to generate an experimental training set, such a reduction translates into fewer samples to generate and test, and thus less money and more time savings. Moreover, important time savings are introduced in numerical simulations, since it would imply less modeling and simulations to run. All these elements help in providing automated and fast estimations of acoustic indicators, which are useful especially for investigating new configurations in preliminary design phases.

Future expansions of the present work may involve the development and implementation of more complex formulations for the description of materials, as well as advanced machine learning techniques, not only for the estimation of the acoustic performance of meta-materials, but even for their choice and optimization, according to the applications of interest. Last, but not least, it has been shown how increasing the number of features leads to an astounding level of accuracy and, at the same time, an appreciable decrease of the number of training examples. These results open the path towards the creation of an

experimental training set, since the limited number of training samples would imply fewer experiments, thus time and money saving.

Author Contributions: Conceptualization, A.C. and D.M.; Data curation, A.C. and D.M.; Investigation, A.C. and D.M.; Methodology, A.C. and D.M.; Resources, D.M.; Supervision, A.C., D.M. and G.P.; Validation, A.C.; Visualization, A.C. and D.M.; Writing—original draft, A.C. and D.M.; Writing—review & editing, G.P., F.F. and S.D.R. All authors have read and agreed to the published version of the manuscript.

Institutional Review Board Statement: Not applicable.

Informed Consent Statement: Not applicable.

Conflicts of Interest: The authors declare no conflict of interest.

References

1. Cao, L.; Fu, Q.; Si, Y.; Ding, B.; Yu, J. Porous materials for sound absorption. *Compos. Commun.* **2018**, *10*, 25–35. [CrossRef]
2. Berardi, U.; Iannace, G. Acoustic characterization of natural fibers for sound absorption applications. *Build. Environ.* **2015**, *94*, 840–852. [CrossRef]
3. Xinzhao, X.; Guoming, L.; Dongyan, L.; Guoxin, S.; Rui, Y. Electrically conductive graphene-coated polyurethane foam and its epoxy composites. *Compos. Commun.* **2018**, *7*, 1–6. [CrossRef]
4. Groby, J.P.; Nennig, B.; Lagarrigue, C.; Brouard, B.; Dazel, O.; Tournat, V. Using simple shape three-dimensional inclusions to enhance porous layer absorption. *J. Acoust. Soc. Am.* **2014**, *136*, 1139–1148. [CrossRef]
5. Yang, Y.; Mace, B.; Kingan, M. Wave and finite element method for predicting sound transmission through finite multi-layered structures with fluid layers. *Comput. Struct.* **2018**, *204*, 20–30. [CrossRef]
6. Weisser, T. Acoustic behavior of a rigidly backed poroelastic layer with periodic resonant inclusions by a multiple scattering approach. *J. Acoust. Soc. Am.* **2016**, *139*, 617–629. [CrossRef] [PubMed]
7. Gaborit, M.; Dazel, O.; Göransson, P. A simplified model for thin acoustic screens. *J. Acoust. Soc. Am.* **2018**, *144*, 76–81. [CrossRef] [PubMed]
8. Groby, J.P.; Wirgin, A.; De Ryck, L.; Lauriks, W.; Gilbert, R.; Xu, Y. Acoustic response of a rigid-frame porous medium plate with a periodic set of inclusions. *J. Acoust. Soc. Am.* **2009**, *126*, 685–693. [CrossRef]
9. Xiong, L.; Nennig, B.; Aurégan, Y.; Bi, W. Sound attenuation optimization using metaporous materials tuned on exceptional points. *J. Acoust. Soc. Am.* **2017**, *142*, 2288–2297. [CrossRef] [PubMed]
10. Yang, M.; Sheng, P. Sound absorption sctructures: From porous media to acoustic metamaterials. *Annu. Rev. Mater. Res.* **2017**, *47*, 83–114. [CrossRef]
11. Veselago, V.G. The electrodynamics of substances with simultaneously negative values of ϵ and μ. *Sov. Phys. Uspekhi* **1968**, *10*, 509–514. [CrossRef]
12. Ma, G.; Sheng, P. Acoustic metamaterials: From local resonances to broad horizons. *Sci. Adv.* **2016**, *2*, e1501595. [CrossRef]
13. Kadic, M.; Bückmann, T.; Schittny, R.; Wegener, M. Metamaterials beyond electromagnetism. *Rep. Prog. Phys.* **2013**, *76*, 126501. [CrossRef] [PubMed]
14. Yang, Z.; Mei, J.; Yang, M.; Chan, N.; Sheng, P. Membrane-type acoustic metamaterial with negative dynamic mass. *Phys. Rev. Lett.* **2008**, *101*, 204301. [CrossRef] [PubMed]
15. Mei, J.; Ma, G.; Yang, M.; Yang, Z.; Wen, W.; Sheng, P. Dark acoustic metamaterials as super absorbers for low-frequency sound. *Nat. Commun.* **2012**, *3*, 756. [CrossRef] [PubMed]
16. Yang, M.; Li, Y.; Meng, C.; Fu, C.; Mei, J.; Yang, Z.; Sheng, P. Sound absorption by subwavelength membrane structures: A geometric perspective. *Comptes Rendus Mec.* **2015**, *343*, 635–644. [CrossRef]
17. Chen, Y.; Huang, C.; Zhou, X.; Hu, G.; Sun, C. Analytical coupled vibroacoustic modeling of membrane-type acustic metamaterials: Membrane model. *J. Acoust. Soc. Am.* **2014**, *136*, 969–979. [CrossRef] [PubMed]
18. Chen, Y.; Huang, C.; Zhou, X.; Hu, G.; Sun, C. Analytical coupled vibroacoustic modeling of membrane-type acustic metamaterials: Plate model. *J. Acoust. Soc. Am.* **2014**, *136*, 2926–2934. [CrossRef] [PubMed]
19. Fang, N.; Xi, D.; Xu, J.; Ambati, M.; Srituravanich, W.; Sun, C.; Zhang, X. Ultrasonic metamaterials with negative modulus. *Nat. Mater.* **2006**, *5*, 452–456. [CrossRef]
20. Wang, X.; Luo, X.; Huang, Z. Ultrathin and durable open metamaterials for simultaneous ventilation and sound reduction. *Appl. Phys. Lett.* **2019**, *115*, 171902-1–171902-5. [CrossRef]
21. Kumar, S.; Xiang, T.; Lee, H. Ventilated acoustic metamaterial window panels for simultaneous noise shielding and air circulation. *Appl. Acoust.* **2020**, *159*, 107088. [CrossRef]

22. Wei, P.; Croënne, C.; Chu, S.; Li, J. Symmetrical and anti-symmetrical coherent perfect absorption for acoustic waves. *Appl. Phys. Lett.* **2014**, *104*, 121902. [CrossRef]
23. Merkel, A.; Theocharis, G.; Richoux, O.; Romero-Garcia, V.; Pagneux, V. Control of acoustic absorption in one-dimensional scattering by resonant scatterers. *Appl. Phys. Lett.* **2015**, *107*, 244102. [CrossRef]
24. Yang, M.; Meng, C.; Fu, C.; Li, Y.; Yang, Z.; Sheng, P. Subwavelength total acoustic absorption with degenerate resonators. *Appl. Phys. Lett.* **2015**, *107*, 104104. [CrossRef]
25. Magliacano, D.; Ouisse, M.; Khelif, A.; De Rosa, S.; Franco, F.; Atalla, N.; Collet, M. Computation of dispersion diagrams for periodic porous materials modeled as equivalent fluids. *Mech. Syst. Signal Process.* **2020**, *142*, 106749. [CrossRef]
26. Magliacano, D.; Ouisse, M.; De Rosa, S.; Franco, F.; Khelif, A. Computation of acoustic properties and design guidelines of periodic Biot-modeled foams. *Appl. Acoust.* **2020**, *168*, 107428. [CrossRef]
27. Magliacano, D.; Ashani, S.; Ouisse, M.; Deckers, E.; Petrone, G.; Desmet, W.; De Rosa, S. Formulation and validation of the shift cell technique for acoustic applications of poro-elastic materials described by the Biot theory. *Mech. Syst. Signal Process.* **2021**, *147*, 107089. [CrossRef]
28. Catapane, G.; Magliacano, D.; Petrone, G.; Casaburo, A.; Franco, F.; De Rosa, S. Transmission Loss Analyses on Different Angular Distributions of Periodic Inclusions in a Porous Layer. *Aerotec. Missili Spazio* **2021**, *100*, 363–373. [CrossRef]
29. Magliacano, D.; Petrone, G.; Franco, F.; De Rosa, S. Numerical investigations about the sound transmission loss of fuselage panel section with embedded periodic foams. *Appl. Acoust.* **2021**, *182*, 108265. [CrossRef]
30. Mitchell, T. *Machine Learning*; McGraw Hill Education: New York, NY, USA, 1997.
31. Bianco, M.; Gerstoft, P.; Traer, J.; Ozanich, E.; Roch, M.; Gannot, S.; Deledalle, C. Machine learning in acoustics: Theory and applications. *J. Acoust. Soc. Am.* **2019**, *146*, 3590–3628. [CrossRef]
32. Michalopoulou, Z.; Gerstoft, P.; Kostek, B.; Roch, M. Introduction to the special issue on machine learning in acoustics. *J. Acoust. Soc. Am.* **2021**, *150*, 3204–3210. [CrossRef]
33. Bacigalupo, A.; Gnecco, G.; Lepidi, M.; Gambarotta, L. Machine-Learning Techniques for the Optimal Design of Acoustic Metamaterials. *J. Optim. Theory Appl.* **2020**, *187*, 630–653. [CrossRef]
34. Gurbuz, C.; Kronowetter, F.; Dietz, C.; Eser, M.; Schmid, J.; Marburg, S. Generative adversarial networks for the design of acoustic metamaterials. *J. Acoust. Soc. Am.* **2021**, *149*, 1162–1174. [CrossRef]
35. Shah, T.; Zhuo, L.; Lai, P.; De La Rosa-Moreno, A.; Amirkulova, F.; Gerstoft, P. Reinforcement learning applied to metamaterial design. *J. Acoust. Soc. Am.* **2021**, *150*, 321–338. [CrossRef]
36. Wu, L.; Liu, L.; Wang, Y.; Zhai, Z.; Zhuang, H.; Krishnaraju, D.; Wang, Q.; Jiang, H. A machine learning-based method to design modular metamaterials. *Extrem. Mech. Lett.* **2020**, *36*, 100657. [CrossRef]
37. Hou, Z.; Tang, T.; Shen, J.; Li, C.; Li, F. Prediction Network of Metamaterial with Split Ring Resonator Based on Deep Learning. *Nanoscale Res. Lett.* **2020**, *15*, 83. [CrossRef]
38. Ciaburro, G.; Iannace, G. Modeling acoustic metamaterials based on reused buttons using data fitting with neural network. *J. Acoust. Soc. Am.* **2021**, *150*, 51–63. [CrossRef]
39. Stender, M.; Adams, C.; Wedler, M.; Grebel, A.; Hoffmann, N. Explainable machine learning determines effects on the sound absorption coefficient measured in the impedance tube. *J. Acoust. Soc. Am.* **2021**, *149*, 1932–1945. [CrossRef]
40. Rasmussen, C.E.; Williams, C.K.I. *Gaussian Processes for Machine Learning*; MIT: Cambridge, MA, USA, 2006.
41. Nabney, I. *Netlab: Algorithms for Pattern Recognition*, 1st ed.; Springer: Berlin, Germany, 2002.
42. Stinson, M. The Propagation Of Plane Sound Waves In Narrow And Wide Circular Tubes, And Generalization To Uniform Tubes Of Arbitrary Cross-Sectional Shape. *J. Acoust. Soc. Am.* **1991**, *89*, 550–558. [CrossRef]
43. Allard, J.; Atalla, N. *Propagation of Sound in Porous Media: Modelling Sound Absorbing Materials*, 2nd ed.; John Wiley and Sons, Ltd.: Hoboken, NJ, USA, 2009; pp. 1–358.
44. Delany, M.; Bazley, E. Acoustical properties of fibrous absorbent materials. *Appl. Acoust.* **1970**, *3*, 105–116. [CrossRef]
45. Miki, Y. Acoustical properties of porous materials: Modifications of Delany-Bazley models. *J. Acoust. Soc. Jpn. (E)* **1990**, *11*, 19–24. [CrossRef]
46. Johnson, D.L.; Koplik, J.; Dashen, R. Theory of dynamic permeability and tortuosity in fluid-saturated porous media. *J. Fluid Mech.* **1987**, *176*, 379. [CrossRef]
47. Champoux, Y.; Allard, J.F. Dynamic tortuosity and bulk modulus in air-saturated porous media. *J. Appl. Phys.* **1991**, *70*, 1975–1979. [CrossRef]
48. Gibbs, M.; MacKay, D. Variational Gaussian process classifiers. *IEEE Trans. Neural Netw.* **2000**, *11*, 1458–1464. [CrossRef]
49. Jaakkola, T.; Haussler, D. Probabilistic kernel regression models. In Proceedings of the Seventh International Workshop on Artificial Intelligence and Statistics, Fort Lauderdale, FL, USA, 3–6 January 1999; Heckerman, D., Whittaker, J., Eds.; PMLR: Cambridge, MA, USA, 1999.
50. Neal, R. Regression and classification using Gaussian process priors. In *Bayesian Statistics 6*; Bernardo, J., Berger, J., Dawid, A., SMith, A., Eds.; Oxford University Press: Oxford, UK, 1998; pp. 475–601.
51. Seeger, M.; Jordan, M. *Sparse Gaussian Process Classification with Multiple Classes*; Technical Report TR 661; Department of Statistics, University of California: Berkeley, CA, USA, 2004.
52. Stein, M.L. *Interpolation of Spatial Data*; Springer: Berlin, Germany, 1999.